Cover Article

EEG Emotion Recognition with Broad Learning System: A Graph Convolutional Residual Framework

Tong Zhang, Qilin Li, and C. L. Philip Chen

***Abstract*—Electroencephalogram (EEG) emotion recognition faces challenges due to the non-Euclidean nature and nonlinear dynamics of EEG signals. Broad learning systems (BLSs), known for fast training and feature expansion, show significant potential in this domain. However, their design limits adaptation to graph-structured EEG data. To address this, a novel framework is introduced, combining BLS with graph convolutional networks (GCNs), realized as GCB-net and Residual GCB-net. BLS drives efficient feature expansion, while GCN modules enhance spatial-temporal feature extraction and model nonlinear EEG dynamics. Residual GCB-net incorporates identity mappings, enabling stable deep network training. Achieving state-of-the-art accuracies of 94.56% on SEED, 91.55% on DREAMER, and 72.20% on MPED, this approach demonstrates resilience to noise and individual variability. This research establishes BLS as a cornerstone for EEG emotion recognition, advancing its application and integration with graph-based models for complex signal analysis. Furthermore, the integration of BLS with GCN offers a promising avenue for the development of more efficient and robust emotion recognition systems, with potential applications in brain-computer interfaces and mental health monitoring.**

***Index Terms*—Broad learning system, electroencephalogram (EEG) emotion recognition, affective computation, graph convolutional network (GCN)**

I. Introduction

ELECTROENCEPHALOGRAM (EEG) emotion recognition aims to determine the emotional state of an individual by analysing EEG signals, offering substantial potential in applications such as human-computer interaction [1], mental health monitoring [2], and affective computing [3]. Notably, this technology can enhance brain-computer interface (BCI) systems, enabling intelligent and user-friendly interactions between users and external devices [4]. Furthermore, in mental health care [5], EEG emotion recognition holds the promise of assisting clinicians in understanding and diagnosing emotional disorders [6] by providing objective insights into the emotional states of patients [7–10]. However, traditional methods for EEG emotion recognition primarily rely on handcrafted feature extraction combined with classifiers such as support vector machines (SVMs) or shallow neural networks [11]. While these approaches have demonstrated moderate success, they are constrained in their ability to model the intricate spatial-temporal relationships and nonlinear dynamics inherent in EEG data [12]. To overcome these limitations, recent advancements [13–15] in deep learning and graph neural networks have emerged, offering transformative methodologies that significantly improve the accuracy and robustness of emotion recognition models. Among these advancements, deep learning architectures, such as convolutional neural networks (CNNs) and recurrent neural networks (RNNs), stand out for their ability to automatically extract hierarchical features from raw EEG data. These models excel at capturing complex patterns and temporal dependencies, ultimately leading to more precise emotional classification. Additionally, graph neural networks, including graph convolutional networks (GCNs), further enhance the field by leveraging the spatial structure of EEG signals, which are naturally represented as graphs through electrode connectivity. By constructing brain networks that capture intricate signal patterns, graph-based methods complement deep learning models and advance emotion recognition accuracy and reliability.

However, despite these technological advancements, several challenges remain. The issue of weak model generalization [16] caused by cross-individual differences persists. Variations in physiological and psychological states between individuals result in differences in EEG signal distribution, limiting the generalization capability of these models across diverse individuals [17]. This is particularly problematic in real-world applications where models need to perform consistently across different populations. Additionally, deep learning models, while powerful, often require extensive computational resources and careful tuning, making them less practical for real-time applications [18]. There is also a need for more efficient frameworks that can handle the noise

Manuscript received: 2 September 2024; revised: 16 November 2024; accepted: 6 February 2025. *(Corresponding author: C. L. Philip Chen.)*

Citation: T. Zhang, Q. Li, and C. L. P. Chen, EEG emotion recognition with broad learning system: A graph convolutional residual framework, *Int. J. Intell. Control Syst.*, 2025, 30(1), 3–15.

Tong Zhang, Qilin Li, and C. L. Philip Chen are with School of Computer Science and Engineering, South China University of Technology, Guangzhou 510006, China, with Research Center for AI Large Models and Intelligent Cognition, Pazhou Lab, Guangzhou 510335, China, and also with Engineering Research Center of the Ministry of Education on Health Intelligent Perception and Paralleled Digital-Human, South China University of Technology, Guangzhou 510006, China (e-mail: tony@scut.edu.cn; qilinli@ieee.org; Philip.chen@ieee.org).

Digital Object Identifier 10.62678/IJICS202506.10158

sensitivity and individual variability prevalent in EEG data while maintaining high accuracy and computational efficiency.

Recent research has shown that feature expansion and incremental learning mechanisms can enhance model adaptability and reduce computational burdens [19]. These approaches not only improve the ability of the model to handle noise and variability in EEG signals but also provide a robust foundation for capturing complex spatial-temporal patterns. Furthermore, integrating advanced graph-based models with efficient learning frameworks has shown promise in addressing the current limitations in EEG emotion recognition [20]. This integration aims to develop more practical and efficient solutions that can better handle the challenges posed by EEG data, moving the field towards more reliable and generalizable emotion recognition systems.

In addition, the application of GCN has demonstrated significant potential in improving the robustness and accuracy of EEG emotion recognition. These networks [21–24] enhance feature extraction by capturing complex spatial-temporal interactions and leveraging residual learning to address issues of gradient vanishing and performance degradation in deep architectures. This approach not only mitigates the impact of individual differences but also improves the adaptability of the model to noisy and variable EEG signals, making it a promising solution for advancing EEG-based emotion recognition. By combining these advancements with broader learning frameworks, the field can move closer to developing systems that are both efficient and capable of handling the inherent complexities of EEG data.

This paper introduces a novel framework that integrates broad learning system (BLS) with graph convolutional broad network (GCB-net) and residual graph convolutional broad network (Residual GCB-net). BLS serves as the backbone for efficient feature expansion and incremental learning, providing a robust foundation for capturing the broad feature space of EEG signals. GCB-net and Residual GCB-net enhance spatial-temporal feature extraction by leveraging the graph-structured nature of EEG data, effectively capturing both local and global patterns. The proposed framework not only addresses the limitations of existing methods but also offers a versatile solution for EEG emotion recognition that is resilient to noise and individual differences. Through comprehensive experiments on benchmark datasets, this study demonstrates the effectiveness and adaptability of the proposed approach, highlighting its potential for practical applications in emotion recognition.

(1) BLS enhances model adaptability and reduces computational burdens through feature expansion and incremental learning. This mechanism allows the model to continuously adapt to new data, making it particularly suitable for handling the noise and variability in EEG signals.

(2) GCB-net leverages graph convolution and regular convolution to effectively capture both local and global patterns in EEG data. By concatenating outputs of all hierarchical layers, GCB-net provides broad searching spaces, enhancing the discriminative capability of the extracted features.

(3) Residual GCB-net addresses issues of gradient vanishing and performance degradation in deep architectures through residual learning. This approach ensures stable training of deeper networks, improving the ability of the model to handle complex spatial-temporal interactions in EEG signals.

II. Related Work

A. BLS Development

Broad learning system has emerged as a promising solution to address the challenges of high-dimensional and large-scale data across various domains. By leveraging efficient feature mapping and enhancement mechanisms, BLS enables rapid model training and adaptation without requiring deep architectures. This section provides a concise overview of the development of BLS and its variants, highlighting their contributions and applications.

The original BLS is introduced by Chen and Liu [25], aiming to provide an efficient learning system without the need for deep architectures. This foundational work lays the groundwork for subsequent variants designed to address specific challenges and enhance performance in diverse applications. Jin et al. propose the regularized BLS [26], which incorporates regularization techniques to improve the generalization performance and stability of the model. Concurrently, Du et al. introduce the recurrent BLS [27], designed to handle sequential data by incorporating recurrent structures, making it suitable for tasks involving time-series information. The year 2019 sees further advancements with the introduction of the convolutional BLS [28] and the ensemble BLS [29]. The convolutional BLS integrates convolutional operations to enhance feature extraction capabilities, particularly for image-related tasks. The ensemble BLS leverages ensemble learning techniques to improve prediction robustness and accuracy by combining multiple BLS models. The gated BLS [27] is proposed to handle complex sequential data through gating mechanisms similar to those in the long short term memory (LSTM) networks, enabling better control over information flow. Additionally, the sequential BLS [30] is developed to process sequential data more efficiently, particularly in applications such as natural language processing. The deep cascade BLS [31] combines the strengths of deep learning and BLS to address complex feature hierarchies, demonstrating significant improvements in tasks requiring deep feature extraction and representation. These variants collectively demonstrate the versatility and adaptability of BLS in addressing diverse challenges across domains such as computer vision, biomedical engineering, control system, and natural language processing. The continuous evolution of BLS research highlights its potential for broader applications and further innovation.

B. GCN-Based EEG Emotion Recognition

GCNs offer a promising solution for EEG emotion recognition by addressing the challenges posed by the non-Euclidean structure and complex spatial-temporal dynamics of EEG signals. Through graph-based representations, GCNs effectively capture the topological relationships and connectivity patterns inherent in EEG data, thereby enhancing the discriminative power of extracted features.

Significant advancements have been made in this domain. Song et al. [32] introduce the dynamical graph convolutional neural network (DGCNN), which dynamically learns the adjacency matrix of EEG channels to uncover intrinsic relationships between electrodes. This method enhances the robustness and accuracy of emotion recognition models by effectively leveraging graph-structured data. Subsequently, Jia et al. [33] propose the channel relationships based graph convolutional network (CR-GCN), which constructs channel relationships using an adjacency matrix that accounts for both local and global interactions among channels. This model demonstrates strong classification performance, achieving average accuracies of 94.69% and 93.95% for valence and arousal in subject-dependent experiments. Li et al. [34] develop the graph-based multi-task self-supervised learning (GMSS) framework, which applies multi-task learning and self-supervised strategies to enhance feature representation. This approach achieves superior performance in semi-supervised EEG emotion recognition tasks. Similarly, Pan et al. [35] propose the multi-scale feature reconstruction graph convolutional network (MSFR-GCN), which incorporates multi-scale feature reconstruction to improve the discriminative power of extracted features. This model achieves notable performance in recognizing emotions using EEG data.

Collectively, these advancements underscore the versatility and adaptability of GCN-based methods in addressing diverse challenges in EEG emotion recognition, including non-Euclidean data structure, individual variability, and noise sensitivity. Moreover, the continuous evolution of GCN-based models highlights their potential for broader applications in affective computing and human-computer interaction.

III. Method and Implementation

This section provides a detailed overview and processes of GCB-net and Residual GCB-net with BLS. Figure 1 illustrates the framework.

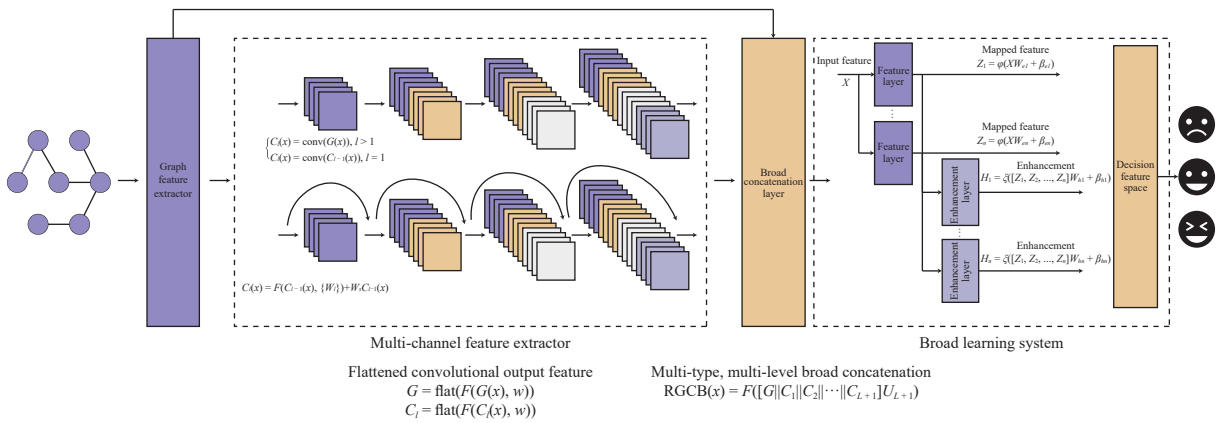

Figure 1 Detailed overview and process of GCB-net and Residual GCB-net with BLS.

A. Broad Learning System

BLS provides an efficient and effective framework for processing large-scale data without resorting to deep architectures, a feature that is particularly beneficial for EEG emotion recognition. In this application, BLS exploits a flat network structure to facilitate rapid training and support incremental learning. The framework comprises two principal components: feature nodes and enhancement nodes. Specifically, feature nodes are produced by projecting the input data into a higher-dimensional space using randomly generated weights and biases, while enhancement nodes further transform these feature nodes to capture more complex patterns. Finally, the output is computed by a linear combination of the feature and enhancement nodes, with the corresponding transformation parameters optimized via the Moore-Penrose pseudoinverse. The process of BLS is illustrated in Fig. 2.

The feature node is generated in Eq. (1)

$$Z_i = \phi(XW_{zi} + \beta_{zi}),\ i = 1, 2, \ldots, n \tag{1}$$

where X is the input data, W_{zi} and β_{zi} are the weight matrix and bias vector, respectively, and ϕ is an activation function.

The enhancement node is computed as

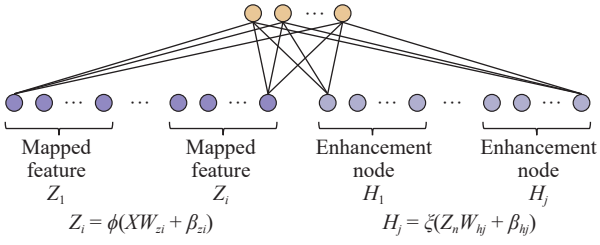

Figure 2 Process of BLS.

$$H_j = \xi(Z_n W_{hj} + \beta_{hj}),\ j = 1, 2, \ldots, m \tag{2}$$

where Z_n is the concatenation of all feature nodes, W_{hj} and β_{hj} are the weight matrix and bias vector for the enhancement nodes, and ξ is a nonlinear activation function.

The final output is given by

$$Y = [Z_n | H_m] W \tag{3}$$

where W is the weight matrix connecting the feature and enhancement nodes to the output layer. The weight matrix W is computed using the pseudoinverse in Eq. (4)

$$W = ([Z_n | H_m]^{\mathrm{T}} [Z_n | H_m] + \lambda I)^{-1} [Z_n | H_m]^{\mathrm{T}} Y \tag{4}$$

where λ is a regularization parameter and I is the identity matrix. To further enhance the efficiency of BLS, ridge regression is employed to approximate the pseudoinverse

$$W = (\lambda I + [Z_n | H_m]^{\mathrm{T}} [Z_n | H_m])^{-1} [Z_n | H_m]^{\mathrm{T}} Y \tag{5}$$

Equation (5) ensures numerical stability and reduces computational complexity. Additionally, BLS supports incremental learning by dynamically expanding feature nodes and enhancement nodes. When new data arrive, the pseudoinverse can be updated incrementally in Eq. (6)

$$W_{\text{new}} = W_{\text{old}} + \Delta W \tag{6}$$

ΔW is computed based on the new data, ensuring that the model adapts efficiently without retraining from scratch.

B. Graph Convolutional Broad Model

Graph convolutional broad represents an innovative integration of GCNs with BLS to enhance feature extraction from graph-structured EEG data for emotion recognition. The data processing process and the graph feature extraction process of GCN are demonstrated in Fig. 3. Initially, the model employs graph convolutional layers to capture the spatial relationships among EEG channels, which are represented as nodes in a graph. These layers utilize the Chebyshev polynomials to approximate spectral filters, enabling efficient computation even on large and complex graphs. Consequently, GCB not only extracts robust spatial features from the EEG signals but also leverages the rapid training and incremental learning capabilities of BLS. This combination significantly improves the discriminative power of the extracted features, thereby advancing the accuracy and reliability of EEG-based emotion classification. The graph convolutional layer is defined as

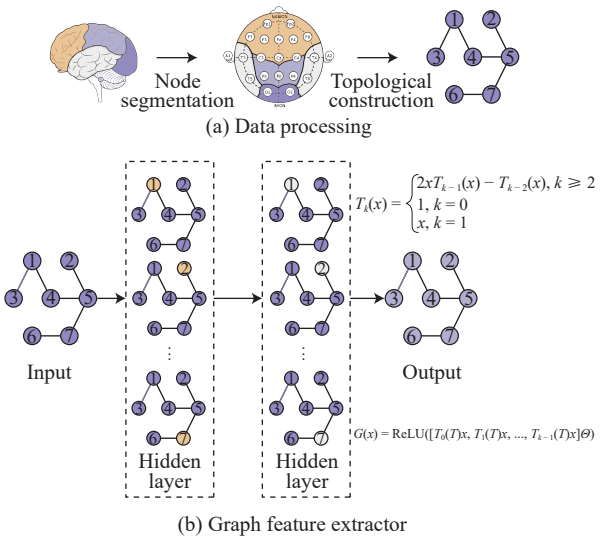

Figure 3 Data processing process and graph feature extraction process of GCN.

$$G(X) = \mathrm{ReLU}\left(\sum_{k=0}^{K-1} T_k(\tilde{L}) X \Theta_k\right) \tag{7}$$

where X is the input data, $T_k(\tilde{L})$ is the Chebyshev polynomial of order k, $\tilde{L} = 2L/\lambda_{\max} - I$ is the normalized graph Laplacian matrix, L is the graph Laplacian, $\lambda_{\max}$ is the maximum eigenvalue of L, and Θ_k is the learnable parameter. The Chebyshev polynomials are recursively computed by Eq. (8)

$$\begin{cases} T_0(x) = 1,\ k = 0; \\ T_1(x) = x,\ k = 1; \\ T_k(x) = 2xT_{k-1}(x) - T_{k-2}(x),\ k \geqslant 2 \end{cases} \tag{8}$$

After the graph convolutional layer, regular convolutional layers are applied to extract higher-level features

$$C_l = \mathrm{conv}(C_{l-1}, h),\ l = 1, 2, \ldots, L \tag{9}$$

where h is the convolutional kernel and L is the number of convolutional layers. The outputs of all layers are concatenated to form the final feature representation

$$\mathrm{GCB}(X) = [G(X); C_1; C_2; \ldots; C_L] \tag{10}$$

To represent EEG features as graph-structured data, an adjacency matrix, A, is constructed based on the connectivity among electrodes. Subsequently, the graph Laplacian, L, is derived from A, which encapsulates the intrinsic structure of the electrode network. Moreover, the Chebyshev polynomial approximation employs the normalized graph Laplacian, $\tilde{L}$, to facilitate efficient spectral filtering and to accurately capture the spatial relationships between EEG channels. Consequently, this methodology effectively models inter-channel dependencies, thereby enhancing the extraction of discriminative features for EEG-based emotion recognition.

The adjacency matrix A is dynamically updated during training to reflect the intrinsic relationships between EEG channels. The update rule for the adjacency matrix is derived from the loss gradient

$$\frac{\partial \mathcal{L}}{\partial A} = \frac{\partial \mathcal{L}}{\partial \tilde{L}} \cdot \frac{\partial \tilde{L}}{\partial A} \tag{11}$$

$$A = (1 - \delta) A + \delta \frac{\partial \mathcal{L}}{\partial A} \tag{12}$$

where δ is the learning rate. This dynamic adjustment of the adjacency matrix allows the model to adapt to the underlying graph structure of the data, enhancing feature extraction capabilities. The adjacency matrix A is updated based on the gradients of the loss function with respect to A. The gradient

computation is performed using backpropagation, allowing the error to propagate from the output layer back through the network to the adjacency matrix. Parameter updates are executed through the Adam optimizer, which dynamically adjusts the learning rate for each parameter based on the magnitude and direction of the gradient. This adaptive optimization strategy improves both the efficiency and stability of the adjacency matrix update process. The graph convolution operation can be further optimized by leveraging the properties of the graph Laplacian.

The integration of graph convolutional layers with conventional convolutional layers in GCB enables the capture of multi-scale features by concurrently addressing the spatial and temporal dimensions of EEG signals. Specifically, the graph convolutional layers are designed to extract spatial interdependencies among EEG channels, effectively modelling the underlying connectivity patterns, while the conventional convolutional layers focus on discerning temporal dynamics inherent in the data. This synergistic combination yields a robust and comprehensive feature representation that is particularly well-suited to the complexities of EEG emotion recognition tasks, thereby enhancing both classification accuracy and overall system reliability.

C. Residual GCB-Net and BLS Optimization

The Residual GCB-net enhances the performance of GCB by incorporating residual learning blocks, which address the vanishing gradient problem in deep networks. Each residual block consists of a residual mapping and an identity mapping, allowing the network to learn deeper features more effectively. The residual block is defined as

$$R(X) = F(X) + X \tag{13}$$

where $F(X)$ is the residual mapping and X is the input to the block. This structure ensures that the network can learn identity mappings more easily, improving the stability and performance of deep architectures. The loss function for Residual GCB-net is defined in Eq. (14)

$$\mathcal{L} = \text{CrossEntropy}(Y, \hat{Y}) + \lambda \|\Theta\|_2^2 \tag{14}$$

where Y denotes the true label, $\hat{Y}$ denotes the predicted label, Θ represents all learnable parameters, and λ is the regularization coefficient. The cross-entropy loss function ensures accurate classification, while L_2 regularization mitigates overfitting. Furthermore, to optimize the Residual GCB-net in conjunction with BLS, the feature extraction process is enhanced by integrating the outputs of residual blocks with the broad learning framework. Specifically, the features extracted by the residual blocks are fed into the BLS, which subsequently generates both feature nodes and enhancement nodes, thereby augmenting the overall representational capacity and robustness of the EEG emotion recognition model. Feature nodes Z_i and enhancement nodes H_j can be represented in Eq. (15)

$$\begin{cases} Z_i = \phi(\text{Residual GCB}(X)W_{zi} + \beta_{zi}), \\ H_j = \xi(Z_n W_{hj} + \beta_{hj}) \end{cases} \tag{15}$$

The final output is computed using the pseudoinverse method as in the standard BLS framework in Eq. (16)

$$W = ([Z_n|H_m]^{\mathrm{T}}[Z_n|H_m] + \lambda I)^{-1}[Z_n|H_m]^{\mathrm{T}} Y \tag{16}$$

The model utilizes residual blocks that capture both local and global features by integrating graph convolutional layers with conventional convolutional layers, as illustrated in Fig. 4. In each block, the graph convolutional layers extract spatial dependencies among EEG channels, while the conventional convolutional layers capture temporal patterns. This multi-scale feature extraction approach yields a comprehensive and discriminative representation that is well-suited to EEG emotion recognition tasks.

The integration of residual learning with BLS capitalizes on the deep feature extraction capabilities of the residual blocks and the efficient learning offered by BLS. Residual blocks facilitate the extraction of progressively deeper features while avoiding gradient vanishing, whereas BLS rapidly expands the feature space through its flat network architecture. This synergistic combination results in enhanced classification accuracy and improved robustness in recognizing emotional states from EEG data.

Moreover, the Residual GCB-net employs a two-stage optimization process in conjunction with the standard BLS optimization. Initially, the graph convolutional layers are trained to discern the spatial relationships among EEG

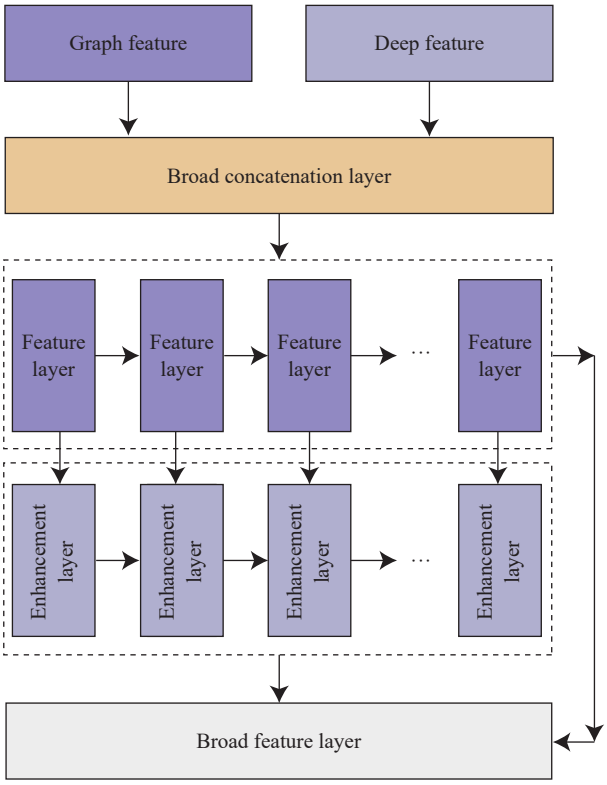

Figure 4 Concatenation process of graph feature and deep feature.

channels. Subsequently, the residual blocks are tuned to extract higher-level features, and finally, the BLS framework refines the representation by optimizing the feature nodes and enhancement nodes. This staged optimization paradigm ensures that each component is effectively trained, thereby leading to superior overall performance in EEG emotion recognition.

IV. Experiment and Analysis

This section evaluates the performance of GCB-net and Residual GCB-net with BLS across three distinct EEG emotion recognition datasets: SEED [36], DREAMER [37], and MPED [38]. Each dataset presents unique challenges and characteristics that influence the selection of appropriate baselines. Specifically, the SEED dataset is designed for discrete emotion classification using multi-channel EEG data, the DREAMER dataset provides continuous ratings of valence, arousal, and dominance, and the MPED dataset incorporates multimodal physiological signals encompassing a broader range of emotions. These intrinsic differences result in variations in the complexity and nature of the EEG signals, as well as in the methodologies and models previously applied to each dataset.

To ensure a fair evaluation, the most relevant and widely reported baselines from the existing literature are selected for comparison. This approach permits a comprehensive assessment of GCB-net and Residual GCB-net with BLS in the context of contemporary EEG emotion recognition methods. Detailed experimental protocols, results, ablation studies, and visualizations of EEG-based emotion recognition are subsequently presented. Collectively, these analyses provide valuable insights into the strengths of GCB-net and Residual GCB-net with BLS in handling diverse emotion recognition tasks, thereby underscoring their potential for advancing the field.

A. EEG Dataset

The SEED, DREAMER, and MPED datasets serve as the basis for evaluating EEG emotion recognition, each offering distinct characteristics. The SEED dataset is designed for three-class classification (positive, neutral, and negative) using EEG recordings from 15 subjects. It provides features such as power spectral density (PSD), differential entropy (DE), differential causality (DCAU), rational asymmetry (RASM), and differential asymmetry (DASM) across specific frequency bands. Emotions are elicited through film clips and recorded with a 62-channel ESI NeuroScan system in conjunction with SMI eye-tracking glasses. In contrast, the DREAMER dataset comprises EEG and electrocardiogram (ECG) recordings from 23 participants exposed to audiovisual stimuli for emotional induction. Participants subsequently self-assess their valence, arousal, and dominance, while EEG data are recorded at 128 Hz using 14 electrodes, with PSD features extracted within the θ, α, and β bands. Furthermore, the MPED dataset focuses on multimodal physiological emotion recognition, incorporating data from 23 subjects that include ECG, electromyography (EMG), galvanic skin response (GSR), and respiration signals recorded in response to various film clips, with EEG data collected using a 62-electrode cap. Collectively, these datasets provide a comprehensive basis for assessing the performance and robustness of EEG emotion recognition systems under diverse experimental conditions.

B. Experimental Implementation

The experimental configuration of GCB-net and Residual GCB-net with BLS is described as follows. The number of EEG channels is determined by the channel configuration of each dataset, and the order of Chebyshev polynomials in the graph convolutional layer is set to 4 to balance computational efficiency with effective feature extraction. The models are trained for 100 epochs with an initial learning rate of 0.004, employing a cosine annealing strategy to facilitate smooth learning rate decay. Moreover, the residual block comprises 9 layers, enhancing the depth and representational capacity of the network. All experiments are conducted on NVIDIA A100 80 GB PCIe graphics processing units, and the entire model is implemented using PyTorch 1.13.0 with CUDA 11.6.

C. Result and Analysis

a. Experiment on SEED

Baseline comparisons evaluate the performance of GCB-net and Residual GCB-net against several models, including SVM, DBN, GCNN, and DGCNN. Table 1 summarizes the accuracy and standard deviation for each model across various frequency bands and feature sets.

The incorporation of BLS markedly enhances GCB-net by expanding the feature space through random mapping and enhancement nodes. For instance, on the DE feature across all frequency bands, GCB-net combined with BLS achieves an accuracy of 94.24% (std 6.70%), compared to 92.30% (std 7.40%) for GCB-net alone. This improvement underscores the capacity of BLS to augment feature representation and mitigate overfitting.

GCB-net effectively captures both spatial and temporal patterns by integrating graph convolutional layers, which model the spatial relationships among EEG channels, with conventional convolutional layers that extract temporal dynamics. For example, on the DE feature within the β band, GCB-net records an accuracy of 88.05% (std 9.84%), thereby outperforming SVM (80.76%) and DBN (78.92%).

Moreover, the incorporation of residual learning in Residual GCB-net further improves performance by addressing the vanishing gradient problem and facilitating deeper feature extraction. According to Table 1, Residual GCB-net achieves higher accuracy than GCB-net across most features and frequency bands. Notably, on the DE feature across all frequency bands, Residual GCB-net attains 92.86% accuracy (std 6.70%), and when combined with BLS, it records the highest accuracy of 94.56% (std 6.61%), thereby demonstrating enhanced feature extraction and model stability.

b. Experiment on DREAMER

The performance of GCB-net and Residual GCB-net is evaluated against several baseline models, including SVM,

Table 1 Comparison of the mean accuracy (ACC)/standard deviation (std) of EEG emotion recognition on SEED.

Feature	Model	δ band		θ band		α band		β band		γ band		All (δ, θ, α, β, and γ)	
		ACC (%)	std (%)	ACC (%)	std (%)	ACC (%)	std (%)	ACC (%)	std (%)	ACC (%)	std (%)	ACC (%)	std (%)
DE	SVM [36]	60.50	14.14	60.95	10.20	66.64	14.41	80.76	11.56	79.56	11.38	83.99	9.72
	DBN [36]	64.32	12.45	60.77	10.42	64.01	15.97	78.92	12.48	79.19	14.58	86.08	8.34
	GCNN [32]	72.75	10.85	74.40	8.23	73.46	12.17	83.24	9.93	83.36	9.43	87.40	9.20
	DGCNN [32]	74.25	11.42	71.52	5.99	74.43	12.16	83.65	10.17	85.73	10.46	90.40	8.49
	GCB-net [39]	80.38	10.04	76.09	7.54	81.36	11.44	88.05	9.84	88.45	9.67	92.30	7.40
	GCB-net + BLS [39]	79.98	8.93	76.51	9.56	81.97	11.05	89.06	8.69	89.10	9.55	94.24	6.70
	Residual GCB-net [39]	80.88	9.04	77.60	7.34	81.95	10.29	88.97	8.50	90.06	9.39	92.86	6.70
	Residual GCB-net + BLS [39]	81.20	7.97	79.85	9.70	84.03	9.93	90.70	7.28	91.70	7.41	94.56	6.61
PSD	SVM [36]	58.03	15.39	57.26	15.09	59.04	15.75	73.34	15.20	71.24	16.38	59.60	15.93
	DBN [36]	60.05	16.66	55.03	13.88	52.79	15.38	60.68	21.31	63.42	19.66	61.90	16.65
	GCNN [32]	69.89	13.83	70.92	9.18	73.18	12.74	76.21	10.76	76.15	10.09	81.31	11.26
	DGCNN [32]	71.23	11.42	71.20	8.99	73.45	12.25	77.45	10.81	76.60	11.83	81.73	9.94
	GCB-net [39]	72.76	12.45	72.31	8.52	74.29	11.22	81.05	12.23	81.85	11.13	83.75	10.63
	GCB-net + BLS [39]	72.90	13.19	74.48	9.03	76.99	10.36	83.30	10.73	83.12	11.95	84.32	10.61
	Residual GCB-net [39]	73.95	11.93	72.42	9.70	74.65	11.49	82.81	11.91	84.12	11.48	84.90	11.53
	Residual GCB-net + BLS [39]	74.38	12.45	75.75	10.16	77.69	12.03	83.55	10.90	83.87	10.96	84.94	10.93
DASM	SVM [36]	48.87	10.49	53.02	12.76	59.81	14.67	75.03	15.72	73.59	16.57	72.81	16.57
	DBN [36]	48.79	9.62	51.59	13.98	54.03	17.05	69.51	15.22	70.06	18.14	72.73	15.93
	GCNN [32]	57.07	6.75	54.80	9.09	62.97	13.43	74.97	13.40	73.28	13.67	76.00	13.32
	DGCNN [32]	55.93	9.14	56.12	7.86	64.27	12.72	73.61	14.35	73.50	16.60	78.45	11.84
	GCB-net [39]	65.04	8.18	65.36	8.97	70.10	11.46	83.22	10.36	83.44	13.21	79.67	14.06
	GCB-net + BLS [39]	62.36	10.66	65.00	10.31	70.91	10.84	85.55	11.39	86.04	10.85	82.09	13.14
	Residual GCB-net [39]	65.48	8.55	66.17	9.97	70.67	11.22	85.45	11.82	84.02	11.36	80.13	12.74
	Residual GCB-net + BLS [39]	66.51	9.41	66.40	10.28	72.12	10.44	86.46	11.45	88.06	10.21	82.25	12.58
RASM	SVM [36]	47.75	10.59	51.40	12.53	60.71	14.57	74.59	16.18	74.61	15.57	74.74	14.79
	DBN [36]	48.05	10.37	50.62	14.02	56.15	15.28	70.31	15.62	68.22	18.09	71.30	16.16
	GCNN [32]	59.70	5.65	55.91	8.82	59.97	14.27	79.45	13.32	79.73	13.22	84.06	12.86
	DGCNN [32]	57.79	6.90	55.79	8.10	61.58	12.63	75.79	13.07	82.32	11.54	85.00	12.47
	GCB-net [39]	62.66	7.22	65.07	8.85	70.79	10.78	85.62	10.11	85.79	12.05	86.40	9.96
	GCB-net + BLS [39]	62.56	8.83	62.22	11.12	71.43	10.83	87.03	11.16	85.59	11.18	87.73	10.19
	Residual GCB-net [39]	66.47	6.88	66.22	8.81	71.71	9.47	86.01	10.53	87.52	10.46	88.98	9.96
	Residual GCB-net + BLS [39]	67.59	7.83	66.42	10.31	74.79	12.35	89.14	10.51	89.24	10.26	90.45	10.22
DCAU	SVM [36]	55.92	14.62	57.16	10.77	61.37	15.97	75.17	15.58	76.44	15.41	77.38	11.98
	DBN [36]	54.58	12.81	56.94	12.54	57.62	13.58	70.70	16.33	72.27	16.12	77.20	14.24
	GCNN [32]	62.60	12.88	65.05	8.35	66.41	11.06	77.28	11.55	78.68	13.00	79.02	11.27
	DGCNN [32]	63.18	13.48	62.55	7.96	67.71	10.74	78.68	10.81	80.05	13.03	81.91	10.06
	GCB-net [39]	70.86	11.27	69.63	9.42	70.66	10.45	82.85	11.65	82.53	11.77	83.32	9.40
	GCB-net + BLS [39]	70.63	10.75	69.82	9.46	73.43	11.38	87.08	9.52	85.56	10.64	86.50	8.63
	Residual GCB-net [39]	72.65	9.27	71.98	10.43	73.53	9.24	85.16	11.08	86.24	12.08	85.00	9.30
	Residual GCB-net + BLS [39]	72.81	11.30	72.26	9.74	74.27	9.91	87.91	9.47	87.70	9.30	87.94	8.59

GraphSLDA, GSCCA, DGCNN, EEGformer, and EmoGT. The results of the EEGformer and EmoGT methods are derived by reproducing the findings reported in Refs. [40, 41] within the framework of this experimental paradigm. The results, as summarized in Table 2, report the mean accuracy and standard deviation for each model across the three emotional dimensions.

GCB-net demonstrates superior performance in capturing both spatial and temporal patterns in EEG data through the integration of graph convolutional layers and conventional convolutional layers. Specifically, the graph convolutional layers effectively model the spatial relationships among EEG channels, while the conventional layers capture the temporal dynamics. Consequently, GCB-net extracts more discriminative features than traditional methods. For example, on the arousal dimension, GCB-net achieves an accuracy of 89.32% with a standard deviation of 5.01%, thereby outperforming both DGCNN (84.54%) and SVM (68.84%).

Besides, the incorporation of residual learning blocks in Residual GCB-net further enhances performance by mitigating the vanishing gradient problem and enabling the extraction of deeper features. The results in Table 2 indicate that Residual GCB-net attains higher accuracy than GCB-net across all emotional dimensions. For instance, on the arousal dimension, Residual GCB-net achieves an accuracy of 91.55% with a standard deviation of 14.78%, compared to 89.32% and 5.01% for GCB-net. This improvement underscores the effectiveness of residual learning in enhancing feature extraction and overall model stability. Specifically, Residual GCB-net with BLS outperforms EEGformer and EmoGT in terms of accuracy across multiple emotional dimensions, highlighting the effectiveness of the proposed framework in capturing complex spatial-temporal patterns in EEG data. This comparison further validates the advanced nature of the proposed method in the context of contemporary EEG emotion recognition techniques.

c. Experiment on MPED

The performance of GCB-net and Residual GCB-net is evaluated against several baseline models, including SVM, DBN, DGCNN, JKNet, and MixHop. Table 3 presents the mean accuracy, standard deviation, and F1-score for each model on both 3-class imbalanced and 7-class emotion recognition tasks.

GCB-net exhibits advanced capability in capturing the intricate spatial and temporal patterns inherent in EEG data by employing a hybrid architecture that integrates graph convolutional layers with conventional convolutional layers. The graph convolutional layers delineate the spatial relationships among EEG channels, while the conventional layers extract temporal dynamics, thereby enabling the extraction of more discriminative features than traditional methods. For example, in the 3-class imbalanced task, GCB-net secures an accuracy of 70.72% (std 7.72%) and an F1-score of 73.95%, surpassing the performance of DGCNN (68.02% accuracy) and SVM (57.06% accuracy).

Furthermore, the incorporation of residual learning blocks in Residual GCB-net further refines feature extraction by alleviating the vanishing gradient problem and permitting the

Table 2 Comparison of ACC/std of EEG emotion recognition on DREAMER.

Model	Valence		Arousal		Dominance	
	ACC (%)	std (%)	ACC (%)	std (%)	ACC (%)	std (%)
SVM [32]	60.14	33.34	68.84	24.94	75.84	20.76
GraphSLDA [32]	57.70	13.89	68.12	17.53	73.90	15.85
GSCCA [32]	56.65	21.50	70.30	18.66	77.31	15.44
DGCNN [32]	86.23	12.29	84.54	10.18	85.02	10.25
GCB-net [39]	86.99	6.21	89.32	5.01	89.20	4.33
EEGformer [40]	88.50	5.50	89.20	4.80	88.80	5.20
EmoGT [41]	87.80	6.30	88.90	5.90	88.50	6.10
Residual GCB-net [39]	87.43	14.89	91.55	14.78	89.37	16.78

Table 3 Comparison of ACC/std/F1-score of EEG emotion recognition on MPED.

Model	3-class imbalanced task			7-class task		
	ACC (%)	std (%)	F1-score (%)	ACC (%)	std (%)	F1-score (%)
SVM [36]	57.06	—	24.43	31.14	8.06	—
DBN [36]	65.98	—	59.19	29.26	9.19	—
DGCNN [32]	68.02	8.81	61.11	36.92	12.78	35.85
JKNet [42]	71.52	9.63	73.15	41.78	10.78	40.52
MixHop [43]	71.15	9.16	72.34	40.02	8.78	42.62
GCB-net [39]	70.72	7.72	73.95	38.88	9.26	38.14
Residual GCB-net [39]	72.20	7.25	74.50	40.67	9.78	40.55

development of deeper representations. As evidenced in Table 3, Residual GCB-net achieves superior performance compared to GCB-net across both tasks. In the 3-class imbalanced scenario, Residual GCB-net attains an accuracy of 72.20% (std 7.25%) and an F1-score of 74.50%, while in the 7-class task, it reaches an accuracy of 40.67% (std 9.78%) and an F1-score of 40.55%, improving upon the corresponding GCB-net metrics. These results confirm that the integration of residual learning optimizes feature extraction and enhances overall model stability in EEG emotion recognition applications.

D. BLS Performance Study

Evaluation of different BLS configurations reveals their impact on EEG emotion recognition tasks. The study compares the standard BLS with stacked BLS [44] by examining accuracy, computational complexity, and generalization performance, with results summarized in Table 4, which presents the accuracy and standard deviation for each configuration across various frequency bands and features.

The standard BLS exhibits superior performance in enhancing feature representation and reducing overfitting through broad feature expansion and random mapping mechanisms. For instance, on the DE feature across all frequency bands, the standard BLS achieves an accuracy of 94.56%, compared to 93.59% for the stacked BLS. Moreover, in terms of computational complexity, the stacked BLS, employing multiple BLS blocks and residual shortcut connections, incurs a complexity that is proportional to the number of blocks, yet this increase does not consistently yield better performance. This suggests that the benefits of the stacked configuration are constrained by both the dataset and the model architecture.

In addition, the standard BLS demonstrates improved generalization performance, as indicated by lower standard deviations across most features and frequency bands. For example, in the γ band of the DE feature, it achieves a standard deviation of 7.41% versus 9.89% for stacked BLS. These findings imply that the standard BLS generalizes more effectively across different subjects and experimental conditions. Furthermore, the performance of stacked BLS appears to be limited by the bottleneck of GCN, as its inherent difficulty in capturing global graph information restricts the potential advantages of additional computational resources. Finally, the limited improvement observed with the stacked BLS underscores the importance of hyperparameter tuning, while adjusting the number of BLS blocks and other parameters may offer incremental gains, the standard BLS remains a more practical choice for EEG emotion recognition tasks given the associated computational overhead.

The performance of stacked BLS appears to be constrained by the inherent limitations of GCN, particularly in its ability to capture global graph information. This restriction diminishes the potential benefits of allocating additional computational resources within the stacked BLS configuration. To address this issue, the proposed framework integrates BLS with GCN, leveraging the extensive feature expansion of BLS alongside the spatial feature extraction capabilities of GCN. This combination enhances the capacity of the model to capture both local and global patterns within EEG data. Moreover, the modest improvements achieved through stacked BLS highlight the critical role of hyperparameter tuning. While modifications to the number of BLS blocks and other parameters may yield incremental enhancements, the standard BLS remains a more pragmatic choice for EEG emotion recognition due to its reduced computational burden. The findings of this study underscore the advantages of standard BLS in terms of accuracy, computational efficiency, and generalization performance,

Table 4 Comparison of BLS types for Residual GCB-net in EEG emotion recognition on SEED dataset.

Feature	Model	δ band		θ band		α band		β band		γ band		All (δ, θ, α, β, and γ)	
		ACC (%)	std (%)	ACC (%)	std (%)	ACC (%)	std (%)	ACC (%)	std (%)	ACC (%)	std (%)	ACC (%)	std (%)
DE	with BLS	81.20	7.97	79.85	9.70	84.03	9.93	90.70	7.28	91.70	7.41	94.56	6.61
	with stacked BLS	79.71	8.54	78.89	9.87	82.59	9.94	90.22	7.35	90.72	9.89	93.59	7.47
PSD	with BLS	74.38	12.45	75.75	10.16	77.69	12.03	83.55	10.90	83.87	10.96	84.94	10.93
	with stacked BLS	72.69	11.66	74.59	10.24	75.99	12.07	83.16	11.28	82.90	12.35	83.23	11.07
DASM	with BLS	66.51	9.41	66.40	10.28	72.12	10.44	86.46	11.45	88.06	10.21	82.25	12.58
	with stacked BLS	65.54	9.00	65.42	10.76	72.36	10.77	86.30	11.17	86.90	10.51	80.49	12.93
RASM	with BLS	67.59	7.83	66.42	10.31	74.79	12.35	89.14	10.51	89.24	10.26	90.45	10.22
	with stacked BLS	67.11	7.95	64.25	11.24	73.11	10.60	88.19	10.28	87.87	10.78	90.17	10.01
DCAU	with BLS	72.81	11.30	72.26	9.74	74.27	9.91	87.91	9.47	87.70	9.30	87.94	8.59
	with stacked BLS	71.91	10.61	71.10	8.17	74.44	9.45	87.57	9.41	86.67	9.36	87.40	8.86

reinforcing its suitability as the foundational component of the proposed EEG emotion recognition framework.

E. Cross-Dataset Study

To comprehensively evaluate the generalization capability of Residual GCB-net in complex and challenging emotion recognition scenarios, cross-dataset comparisons are conducted within the SEED family of datasets. For the cross-dataset comparison between SEED and SEED-V, the emotions of happy, neutral, and a combination of disgust, fear, and sadness in SEED-V correspond to the positive, neutral, and negative emotions of SEED, respectively. As indicated in Table 5, under the scenario of class imbalance across datasets, Residual GCB-net achieves superior recognition performance, with an accuracy of 58.83% when transferring from SEED to SEED-V and an accuracy of 49.43% when transferring from SEED-V back to SEED. The increased diversity among subjects introduces additional challenges in cross-dataset experiments, however, Residual GCB-net demonstrates improved transfer effectiveness compared to alternative methods, further validating its robustness and adaptability in emotion recognition tasks.

F. Residual Block Layer Robustness Study

The performance of Residual GCB-net is evaluated with varying numbers of residual blocks to assess the impact of network depth on EEG emotion recognition accuracy. Experiments conducted on the SEED dataset yield accuracy and standard deviation for each model configuration across multiple frequency bands and feature sets, as summarized in Table 6.

The results reveal that performance varies with the number of residual blocks. Notably, the 9-layer Residual GCB-net attains the highest accuracy, achieving 92.86% with a standard deviation of 6.70% on the DE feature across all frequency bands. This configuration demonstrates superior performance across most frequency bands. For example, in the β band, the 9-layer model achieves 88.97% accuracy, outperforming both the 6-layer model and the 12-layer model.

Furthermore, the findings indicate that increasing the number of residual blocks initially enhances performance, but excessive network depth ultimately introduces noise and redundant features, leading to a decline in accuracy. The 9-layer configuration strikes an optimal balance between model complexity and performance by effectively capturing critical spatial and temporal patterns without overfitting. In contrast, the 15-layer model records a slightly lower accuracy of 92.78%, confirming that an optimal network depth is crucial for robust EEG emotion recognition performance.

G. Analysis of Discriminative Representation

Figure 5 utilizes the t-distributed stochastic neighbor embedding (t-SNE) method to visualize the learned feature space, demonstrating the capacity of the Residual GCB-net to

Table 5 Comparison of ACC of EEG emotion recognition between SEED and SEED-V datasets.

Method	ACC (%)	
	SEED→SEED-V	SEED-V→SEED
IAG [45]	57.09	40.58
GMSS [34]	58.11	46.06
DDC [46]	54.97	34.34
DAN [47]	57.98	43.34
MS-MDA [48]	55.74	40.67
UDDA [49]	58.17	41.06
Residual GCB-net [14]	58.83	49.43

Table 6 Comparison of Residual GCB-net with different layers for EEG emotion recognition on SEED dataset (DE).

Model	δ band		θ band		α band		β band		γ band		All (δ, θ, α, β, and γ)	
	ACC (%)	std (%)	ACC (%)	std (%)	ACC (%)	std (%)	ACC (%)	std (%)	ACC (%)	std (%)	ACC (%)	std (%)
9-layer Residual GCB-net	80.88	9.04	77.60	7.34	81.95	10.29	88.97	8.50	90.06	9.39	92.86	6.70
6-layer Residual GCB-net	79.41	8.90	75.39	7.28	79.62	12.07	87.61	9.21	89.00	9.47	92.72	6.83
9-layer-all-concatenate Residual GCB-net	79.59	9.06	77.83	8.65	80.26	11.25	87.58	8.88	88.56	8.93	91.75	8.13
12-layer Residual GCB-net	78.50	10.08	75.45	6.45	78.86	12.49	89.10	8.70	88.57	8.48	92.94	6.58
15-layer Residual GCB-net	80.39	9.39	76.20	7.91	80.78	10.76	88.65	10.31	89.48	10.07	92.78	6.41

extract patterns and structures in EEG data associated with different emotions. Figure 5(a) shows that raw EEG features result in scattered and indistinct clusters, reflecting a lack of discernible patterns. After training with the Residual GCB-net, Fig. 5(b) depicts a substantial improvement, with points clearly forming three distinct clusters corresponding to negative, neutral, and positive emotions.

The t-SNE visualizations highlight the ability of the Residual GCB-net to enhance feature separability and achieve effective emotion classification. Despite some mixed points, the clear separation of clusters in the trained feature space demonstrates the robustness of the model in leveraging EEG data. This conclusion is further reinforced by discriminative representation analysis, which indicates enhanced generalization across emotional dimensions. These results underscore the potential of the model for practical applications in continuous emotion recognition through its effective capture of spatial and temporal EEG patterns.

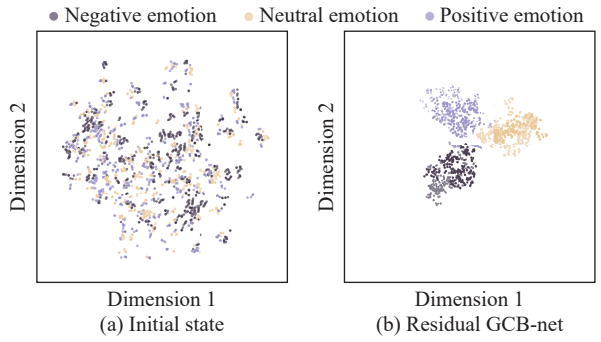

Figure 5 t-SNE visualization of the feature extracted by Residual GCB-net on SEED using the DE feature from all frequency bands.

V. Conclusion

In conclusion, this study presents an innovative framework that integrates BLS with GCNs through GCB-net and Residual GCB-net architectures, effectively addressing the challenges associated with the non-Euclidean structure and nonlinear dynamics of EEG signals in emotion recognition. By leveraging the rapid feature expansion and incremental learning capabilities of BLS in conjunction with the ability of GCN to model spatial-temporal dependencies and electrode connectivity, the framework achieves state-of-the-art accuracies of 94.56% on SEED, 91.55% on DREAMER, and 72.20% on MPED, outperforming existing methods such as DGCNN and SVM/DBN baselines. The incorporation of residual learning stabilizes deep network architectures, mitigates the vanishing gradient problem, and enhances robustness against noise and cross-subject variability. Additionally, the dynamic refinement of adjacency matrices allows for the adaptive modelling of intrinsic EEG channel relationships, further improving the ability of the framework to capture complex dependencies within the data. These advancements not only deepen the theoretical understanding of graph-based EEG feature extraction but also position BLS as a computationally efficient and effective backbone for real-world affective computing applications. Future research will focus on extending this framework to include multimodal physiological signals and developing lightweight variants tailored for edge computing. This will involve measuring computational resource consumption indicators like floating point operations per second (FLOPs) and memory usage to facilitate more comprehensive comparisons with other models. Such explorations aim to bridge the gap between achieving high accuracy and ensuring practical deployability in brain-computer interface systems, paving the way for broader applications in emotion recognition and beyond.

Future research will focus on enhancing cross-dataset generalization through domain adaptation techniques to address discrepancies in EEG signal distributions across datasets such as SEED and DREAMER. Additionally, integrating multimodal physiological signals, including EEG, ECG, and GSR, via a feature alignment mechanism will improve feature representation and robustness in emotion recognition. To ensure real-time applicability in resource-constrained environments, lightweight model variants will be explored, with knowledge distillation based compression enabling efficient deployment without significant accuracy loss. These advancements will strengthen the adaptability and scalability of the framework for practical applications in affective computing.

Acknowledgment

This work was supported by the National Natural Science Foundation of China (No. 62222603), the STI2030-Major Projects grant from Ministry of Science and Technology of the People's Republic of China (No. 2021ZD0200700), the Key-Area Research and Development Program of Guangdong Province (No. 2023B0303030001), the Program for Guangdong Introducing Innovative and Entrepreneurial Teams (No. 2019ZT08X214), and the Science and Technology Program of Guangzhou (No. 2024A04J6310).

References

[1] K. Xia, W. Duch, Y. Sun, K. Xu, W. Fang, H. Luo, Y. Zhang, D. Sang, X. Xu, F.-Y. Wang et al., Privacy-preserving brain-computer interfaces: A systematic review, *IEEE Trans. Comput. Soc. Syst.*, 2023, 10(5), 2312–2324.

[2] C. Cheng, Z. Yu, Y. Zhang, and L. Feng, Hybrid network using dynamic graph convolution and temporal self-attention for EEG-based emotion recognition, *IEEE Trans. Neural Netw. Learning Syst.*, 2024, 35(12), 18565–18575.

[3] T. Zhang, Q. Li, J. Wen, and C. L. Philip Chen, Enhancement and optimisation of human pose estimation with multi-scale spatial attention and adversarial data augmentation, *Inf. Fusion*, 2024, 111, 102522.

[4] X. Xu, T. Jia, Q. Li, F. Wei, L. Ye, and X. Wu, EEG feature selection via global redundancy minimization for emotion recognition, *IEEE Trans. Affect. Comput.*, 2023, 14(1), 421–435.

[5] W. Zheng, L. Yan, and F.-Y. Wang, Two birds with one stone: Knowledge-embedded temporal convolutional transformer for depression detection and emotion recognition, *IEEE Trans. Affect. Comput.*, 2023, 14(4), 2595–2613.

[6] H. Rehman, D. M. Khan, H. Amanullah, L. Kamran, O. U. Rehman, S.

T. Siddiqui, and K. Masroor, Advances in EEG-based detection of major depressive disorder using shallow and deep learning techniques: A systematic review, *Comput. Biol. Med.*, 2025, 192, 110154.

[7] L. Pepa, L. Spalazzi, M. Capecci, and M. G. Ceravolo, Automatic emotion recognition in clinical scenario: A systematic review of methods, *IEEE Trans. Affect. Comput.*, 2023, 14(2), 1675–1695.

[8] M. Egger, M. Ley, and S. Hanke, Emotion recognition from physiological signal analysis: A review, *Electron. Notes Theor. Comput. Sci.*, 2019, 343, 35–55.

[9] S. K. B. Sangeetha, R. R. Immanuel, S. K. Mathivanan, J. Cho, and S. V. Easwaramoorthy, An empirical analysis of multimodal affective computing approaches for advancing emotional intelligence in artificial intelligence for healthcare, *IEEE Access*, 2024, 12, 114416–114434.

[10] G. Amrani, A. Adadi, M. Berrada, Z. Souirti, and S. Boujraf, EEG signal analysis using deep learning: A systematic literature review, in *Proc. 2021 Fifth International Conference On Intelligent Computing in Data Sciences*, Fez, Morocco, 2021, 1–8.

[11] W. Tao, C. Li, R. Song, J. Cheng, Y. Liu, F. Wan, and X. Chen, EEG-based emotion recognition via channel-wise attention and self attention, *IEEE Trans. Affect. Comput.*, 2023, 14(1), 382–393.

[12] W. Cai, H. Sun, R. Liu, Y. Cui, J. Wang, Y. Xia, D. Yao, and D. Guo, A spatial-channel-temporal-fused attention for spiking neural networks, *IEEE Trans. Neural Netw. Learn. Syst.*, 2024, 35(10), 14315–14329.

[13] G. Du, S. Long, C. Li, Z. Wang, and P. Liu, A product fuzzy convolutional network for detecting driving fatigue, *IEEE Trans. Cybern.*, 2023, 53(7), 4175–4188.

[14] B. Chen, C. L. P. Chen, and T. Zhang, Ugan: Uncertainty-guided graph augmentation network for EEG emotion recognition, *IEEE Trans. Comput. Soc. Syst.*, 2025, 12(2), 695–707.

[15] C. Su, Z. Xu, J. Pathak, and F. Wang, Deep learning in mental health outcome research: A scoping review, *Transl. Psychiatry*, 2020, 10(1), 116.

[16] H. Chen, S. Sun, J. Li, R. Yu, N. Li, X. Li, and B. Hu, Personal-zscore: Eliminating individual difference for EEG-based cross-subject emotion recognition, *IEEE Trans. Affect. Comput.*, 2023, 14(3), 2077–2088.

[17] J. Li, S. Qiu, Y.-Y. Shen, C.-L. Liu, and H. He, Multisource transfer learning for cross-subject EEG emotion recognition, *IEEE Trans. Cybern.*, 2020, 50(7), 3281–3293.

[18] R. Zhou, W. Ye, Z. Zhang, Y. Luo, L. Zhang, L. Li, G. Huang, Y. Dong, Y.-T. Zhang, and Z. Liang, EEGMatch: Learning with incomplete labels for semisupervised EEG-based cross-subject emotion recognition, *IEEE Trans. Neural Netw. Learn. Syst*., to be published.

[19] M. Jiménez-Guarneros and R. Alejo-Eleuterio, A class-incremental learning method based on preserving the learned feature space for EEG-based emotion recognition, *Mathematics*, 2022, 10(4), 598.

[20] L. Galluccio, L. D'Errico, M. Giordano, and M. Staffa, Advancing EEG-based emotion recognition: Unleashing the power of graph neural networks for dynamic and topology-aware models, in *Proc. 2024 International Joint Conference on Neural Networks*, Yokohama, Japan, 2024, 1–8.

[21] F. Zheng, B. Hu, S. Zhang, Y. Li, and X. Zheng, EEG emotion recognition based on hierarchy graph convolution network, in *Proc. 2021 IEEE International Conference on Bioinformatics and Biomedicine*, Houston, TX, USA, 2021, 1628–1632.

[22] C. Li, T. Tang, Y. Pan, L. Yang, S. Zhang, Z. Chen, P. Li, D. Gao, H. Chen, F. Li et al., An efficient graph learning system for emotion recognition inspired by the cognitive prior graph of EEG brain network, *IEEE Trans. Neural Netw. Learn. Syst.*, 2025, 36(4), 7130–7144.

[23] C. Li, P. Li, Z. Chen, L. Yang, F. Li, F. Wan, Z. Cao, D. Yao, B.-L. Lu, and P. Xu, Brain network manifold learned by cognition-inspired graph embedding model for emotion recognition, *IEEE Trans. Syst., Man, Cybern.: Syst.*, 2024, 54(12), 7794–7808.

[24] J. M. Górriz, I. Álvarez-Illán, A. Álvarez-Marquina, J. E. Arco, M. Atzmueller, F. Ballarini, E. Barakova, G. Bologna, P. Bonomini, G. Castellanos-Dominguez et al., Computational approaches to explainable artificial intelligence: Advances in theory, applications and trends, *Inf. Fusion*, 2023, 100, 101945.

[25] C. L. P. Chen and Z. Liu, Broad learning system: An effective and efficient incremental learning system without the need for deep architecture, *IEEE Trans. Neural Netw. Learn. Syst.*, 2018, 29(1), 10–24.

[26] J. Jin, Z. Liu, and C. L. Philip Chen, Discriminative graph regularized broad learning system for image recognition, *Sci. China Inf. Sci.*, 2018, 61(11), 112209.

[27] J. Du, C.-M. Vong, and C. L. Philip Chen, Novel efficient RNN and LSTM-like architectures: Recurrent and gated broad learning systems and their applications for text classification, *IEEE Trans. Cybern.*, 2021, 51(3), 1586–1597.

[28] C. L. Philip Chen, Z. Liu, and S. Feng, Universal approximation capability of broad learning system and its structural variations, *IEEE Trans. Neural Netw. Learn. Syst.*, 2019, 30(4), 1191–1204.

[29] X.-N. Fan and S.-W. Zhang, LPI-BLS: Predicting lncRNA-protein interactions with a broad learning system-based stacked ensemble classifier, *Neurocomputing*, 2019, 370, 88–93.

[30] S.-C. Kuok and K.-V. Yuen, Model-free data reconstruction of structural response and excitation via sequential broad learning, *Mech. Syst. Signal Process.*, 2020, 141, 106738.

[31] H. Ye, H. Li, and C. L. Philip Chen, Adaptive deep cascade broad learning system and its application in image denoising, *IEEE Trans. Cybern.*, 2021, 51(9), 4450–4463.

[32] T. Song, W. Zheng, P. Song, and Z. Cui, EEG emotion recognition using dynamical graph convolutional neural networks, *IEEE Trans. Affect. Comput.*, 2020, 11(3), 532–541.

[33] J. Jia, B. Zhang, H. Lv, Z. Xu, S. Hu, and H. Li, CR-GCN: Channel-relationships-based graph convolutional network for EEG emotion recognition, *Brain Sci.*, 2022, 12(8), 987.

[34] Y. Li, J. Chen, F. Li, B. Fu, H. Wu, Y. Ji, Y. Zhou, Y. Niu, G. Shi, and W. Zheng, GMSS: Graph-based multi-task self-supervised learning for EEG emotion recognition, *IEEE Trans. Affect. Comput.*, 2023, 14(3), 2512–2525.

[35] D. Pan, H. Zheng, F. Xu, Y. Ouyang, Z. Jia, C. Wang, and H. Zeng, MSFR-GCN: A multi-scale feature reconstruction graph convolutional network for EEG emotion and cognition recognition, *IEEE Trans. Neural Syst. Rehabil. Eng.*, 2023, 31, 3245–3254.

[36] W.-L. Zheng and B.-L. Lu, Investigating critical frequency bands and channels for EEG-based emotion recognition with deep neural networks, *IEEE Trans. Auton. Mental Dev.*, 2015, 7(3), 162–175.

[37] S. Katsigiannis and N. Ramzan, DREAMER: A database for emotion recognition through EEG and ECG signals from wireless low-cost off-the-shelf devices, *IEEE J. Biomed. Health Inf.*, 2018, 22(1), 98–107.

[38] T. Song, W. Zheng, C. Lu, Y. Zong, X. Zhang, and Z. Cui, MPED: A multi-modal physiological emotion database for discrete emotion recognition, *IEEE Access*, 2019, 7, 12177–12191.

[39] Q. Li, T. Zhang, C. L. Philip Chen, K. Yi, and L. Chen, Residual GCB-Net: Residual graph convolutional broad network on emotion recognition, *IEEE Trans. Cogn. Dev. Syst.*, 2023, 15(4), 1673–1685.

[40] Y. Song, Q. Zheng, B. Liu, and X. Gao, EEG conformer: Convolutional transformer for EEG decoding and visualization, *IEEE Trans. Neural Syst. Rehabil. Eng.*, 2023, 31, 710–719.

[41] W.-B. Jiang, X. Yan, W.-L. Zheng, and B.-L. Lu, Elastic graph

transformer networks for EEG-based emotion recognition, in *Proc. 2023 IEEE International Conference on Acoustics, Speech and Signal Processing*, Rhodes Island, Greece, 2023, 1–5.

[42] K. Xu, C. Li, Y. Tian, T. Sonobe, K.-I. Kawarabayashi, and S. Jegelka, Representation learning on graphs with jumping knowledge networks, in *Proc. 35th International Conference on Machine Learning*, Stockholm, Sweden, 2018, 5453–5462.

[43] S. Abu-El-Haija, B. Perozzi, A. Kapoor, N. Alipourfard, K. Lerman, H. Harutyunyan, G. Ver Steeg, and A. Galstyan, MixHop: Higher-order graph convolutional architectures via sparsified neighborhood mixing, in *Proc. 36th International Conference on Machine Learning*, Long Beach, CA, USA, 2019, 21–29.

[44] Z. Liu, C. L. Philip Chen, S. Feng, Q. Feng, and T. Zhang, Stacked broad learning system: From incremental flatted structure to deep model, *IEEE Trans. Syst., Man, Cybern.: Syst.*, 2021, 51(1), 209–222.

[45] T. Song, S. Liu, W. Zheng, Y. Zong, and Z. Cui, Instance-adaptive graph for EEG emotion recognition, in *Proc. 34th AAAI Conference on Artificial Intelligence*, New York, NY, USA, 2020, 2701–2708.

[46] E. Tzeng, J. Hoffman, N. Zhang, K. Saenko, and T. Darrell, Deep domain confusion: Maximizing for domain invariance, arXiv preprint arXiv: 1412.3474, 2014.

[47] H. Li, Y.-M. Jin, W.-L. Zheng, and B.-L. Lu, Cross-subject emotion recognition using deep adaptation networks, in *Proc. 25th International Conference on Neural Information Processing*, Siem Reap, Cambodia, 2018, 403–413.

[48] H. Chen, M. Jin, Z. Li, C. Fan, J. Li, and H. He, MS-MDA: Multisource marginal distribution adaptation for cross-subject and cross-session EEG emotion recognition, *Front. Neurosci.*, 2021, 15, 778488.

[49] Z. Li, E. Zhu, M. Jin, C. Fan, H. He, T. Cai, and J. Li, Dynamic domain adaptation for class-aware cross-subject and cross-session EEG emotion recognition, *IEEE J. Biomed. Health Inf.*, 2022, 26(12), 5964–5973.

Tong Zhang received the BS degree in software engineering from Sun Yat-sen University, Guangzhou, China, in 2009, the MS degree in applied mathematics from University of Macau, Macao, China, in 2011, and the PhD degree in software engineering from University of Macau, Macao, China, in 2016. He is currently a professor and associate dean at School of Computer Science and Engineering, South China University of Technology, China. He is an associate editor of *IEEE Transactions on Affective Computing*, *IEEE Transactions on Computational Social Systems*, and *Journal of Intelligent Manufacturing*. He has been working in publication matters for many IEEE conferences. His research interests include affective computing, evolutionary computation, neural network, and other machine learning techniques and their applications.

Qilin Li received the BEng degree in electrical engineering and automation from Wuhan University of Science and Technology, Wuhan, China, in 2018, and the MS degree in computer science from University of Wollongong, Wollongong, Australia, in 2020. He is currently pursuing the PhD degree in computer science and technology at School of Computer Science and Engineering, South China University of Technology, Guangzhou, China. His research interests include affective computing and neural network.

C. L. Philip Chen received the MS degree in electrical and computer science from University of Michigan at Ann Arbor, Ann Arbor, MI, USA, in 1985, and the PhD degree in electrical and computer science from Purdue University, West Lafayette, USA, in 1988. He is currently the chair professor and the dean at School of Computer Science and Engineering, South China University of Technology, Guangzhou, China. Being a program evaluator of the Accreditation Board of Engineering and Technology Education, USA, for computer engineering, electrical engineering, and software engineering programs, he successfully architected the engineering and computer science programs of University of Macau, China, receiving accreditations from Washington/Seoul Accord through Hong Kong Institute of Engineers (HKIE), Hong Kong, China, of which is considered as his utmost contribution in engineering/computer science education for Macao as the former dean of the Faculty of Science and Technology, University of Macau, China. His research interests include cybernetics, systems, and computational intelligence. He was a recipient of the 2016 Outstanding Electrical and Computer Engineers Award from Purdue University in 1988. He received the IEEE Norbert Wiener Award in 2018 for his contribution in systems and cybernetics, and machine learning. He is also a highly cited researcher by Clarivate Analytics in 2018, 2019, and 2020. He is currently the editor-in-chief of the *IEEE Transactions on Cybernetics*, an associate editor of the *IEEE Transactions on Artificial Intelligence*, and *IEEE Transactions on Fuzzy Systems*. He was the IEEE Systems, Man, and Cybernetics Society president from 2012 to 2013, the editor-in-chief of the *IEEE Transactions on Systems, Man, and Cybernetics: Systems* from 2014 to 2019. He was the chair of TC 9.1 Economic and Business Systems of International Federation of Automatic Control from 2015 to 2017. He is a fellow of AAAS, IAPR, Chinese Association of Automation, and HKIE, a member of Academia Europaea and European Academy of Sciences and Arts.